# Hypervelocity impact performance of open cell foam core sandwich panel structures

S. Ryan [*,1], E Ordonez[2], E.L. Christiansen[3], D.M. Lear[3]
[1]USRA Lunar and Planetary Institute, 3600 Bay Area Blvd, Houston, TX, 77058, USA
[2]MEI Technologies Inc/ESCG, 2224 Bay Area Blvd, Houston, TX, 77058, USA
[3]NASA Johnson Space Center, 2101 NASA Pkwy, Houston, TX, 77058, USA

Received 15 December 2009; received in revised form 17 March 2010; accepted 6 September 2010

**Abstract**

Open cell metallic foam core sandwich panel structures are of interest for application in spacecraft micrometeoroid and orbital debris shields due to their novel form and advantageous structural and thermal performance. Repeated shocking as a result of secondary impacts upon individual foam ligaments during the penetration process acts to raise the thermal state of impacting projectiles, resulting in fragmentation, melting, and vaporization at lower velocities than with traditional shielding configurations (e.g. Whipple shield). In order to characterize the protective capability of these structures, an extensive experimental campaign was performed by the Johnson Space Center Hypervelocity Impact Technology Facility, the results of which are reported in this paper. Although not capable of competing against the protection levels achievable with leading heavy shields in use on modern high-risk vehicles (i.e. International Space Station modules), metallic foam core sandwich panels are shown to provide a substantial improvement over comparable structural panels and traditional low weight shielding. A ballistic limit equation, generalized in terms of panel geometry, is derived and presented in a form suitable for application in risk assessment codes.

*Keywords*: Hypervelocity impact, orbital debris, space environment, cellular materials

## 1. Introduction

Mission restrictions (e.g. weight, launch volume, etc.) often prevent the inclusion of a dedicated protective structure for space vehicles against micrometeoroid and orbital debris (MMOD) impact. In such cases, the vehicle primary structure acts as the de facto shield. As a result, honeycomb sandwich panels with aluminum or composite facesheets are amongst the most common MMOD shields, despite being unsuited to this task. For impacts in which generated pressures are sufficient to induce projectile fragmentation, the presence of the honeycomb cell walls acts to limit the expansion of the debris cloud as it propagates through the thickness of the panel core, a phenomenon commonly referred to as

*Corresponding author. Tel.: +1 281 483-2983; fax: +1 281 483-3908.
*E-mail address:* shannon.j.ryan@nasa.gov

channeling (e.g. 0). Metallic foams are a relatively new class of materials with low density and novel physical, mechanical, thermal, electrical and acoustic properties. Although incompletely characterized, they offer comparable mechanical performance to traditional spacecraft primary structures without features detrimental to MMOD shielding (i.e. through-thickness channeling cells). There are two competing types of metallic foams: open cell and closed cell. Open cell foams are considered the more promising technology due to their lower weight and higher degree of homogeneity. Preliminary investigations of open cell metallic foam under hypervelocity impact (e.g. 00) have identified the potential of this material in MMOD shielding.

The performance of metallic open cell foam core sandwich panels has been the subject of a recent investigation at NASA Johnson Space Center's Hypervelocity Impact Technology Facility (HITF). In this paper, the results of this experimental program are reported, and the applicability of metallic foam core sandwich panel structures to MMOD shielding is evaluated.

## 2. Description of the Investigated Material

For this study, Duocel© open cell aluminum foams from ERG Aerospace have been selected for testing. Duocel foams are manufactured through utilization of a solid negative-image ceramic mould, which is filled with a liquid aluminum alloy and allowed to cool. The individual cells are typically 14-faceted polyhedral or solid tetrakaidecahedrons. Once the foam has solidified, the thin membranes or windows are removed through a reticulation process, leaving behind only interconnected struts which form the open-cell structure. The tetrakaidecahedrons are referred to as cells, and the individual windows between the interconnected foam ligaments are the pores, shown in Fig. 1. The pore size controls the number and nominal size of foam ligaments, while the foam relative density controls their cross-sectional form and actual size. Examples of ligament cross-sections are also provided in Fig. 1.

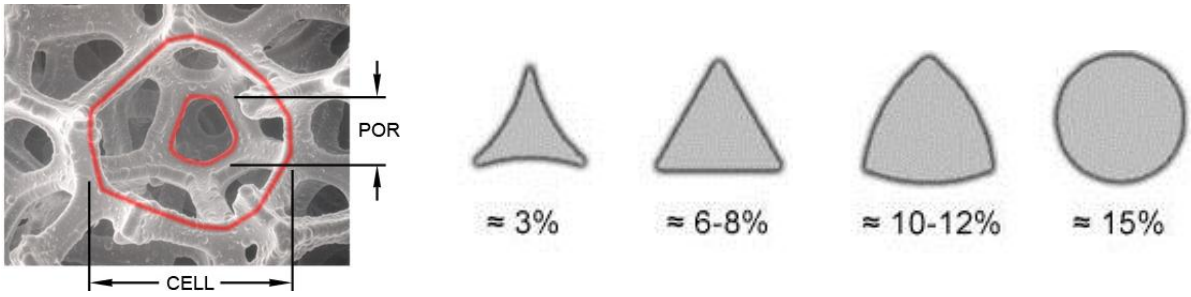


Fig. 1. Open cell foam pore and cell size (left), and ligament cross section variation with relative density (© ERG Aerospace).

## 3. Impact Testing

A total of 98 hypervelocity impact tests have been performed on the open cell foam core sandwich panels over a range of impact angles (0°/45°/60°) and velocities (2.18-7.56 km/s). The performance of panels with varying pore densities (10/20/40 PPI), core (12.7/25.4/50.8 mm) and facesheet (0.254/0.381/0.508 mm) thicknesses, and pore densities (3-5% / 6-8%) have been evaluated. The experimental setup is shown in Fig. 2. An overview of the test configurations is given in Table 1.

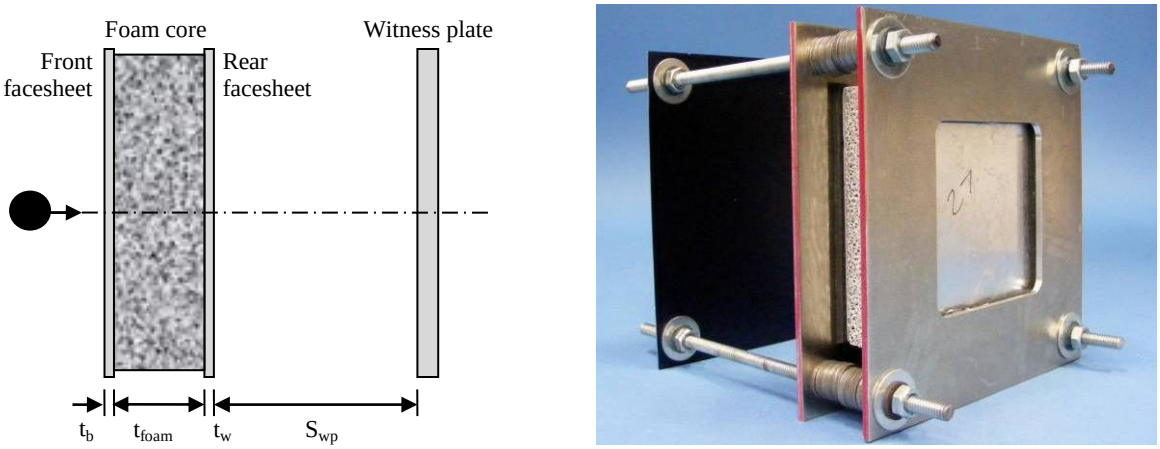


Fig. 2. Schematic (left) and pre-test photograph (right) of the experimental setup.

Table 1. Overview of target configurations

| | *Front facesheet* | | *Rear facesheet* | | | *Core* | *Total* |
|---|---|---|---|---|---|---|---|
| *Type* | *Material* | *Thickness (cm)* | *Material* | *Thickness (cm)* | *Pore density (PPI)* | *Thickness (cm)* | *AD ($g/cm^3$)* |
| 1.0” Al F10 | Al6061-T6 | 0.0254 | Al6061-T6 | 0.0254 | 10 | 2.54 | 0.79 |
| 1.0” Al F20 | Al6061-T6 | 0.0254 | Al6061-T6 | 0.0254 | 20 | 2.54 | 0.77 |
| 1.0” Al F40 | Al6061-T6 | 0.0254 | Al6061-T6 | 0.0254 | 40 | 2.54 | 0.78 |
| 0.5” Al F10 | Al6061-T6 | 0.0254 | Al6061-T6 | 0.0254 | 10 | 1.27 | 0.51 |
| 0.5” Al F40 | Al6061-T6 | 0.0254 | Al6061-T6 | 0.0254 | 40 | 1.27 | 0.49 |
| 2.0” Al F10 | Al6061-T6 | 0.0254 | Al6061-T6 | 0.0254 | 10 | 5.08 | 1.25 |
| 2.0” Al F40 | Al6061-T6 | 0.0254 | Al6061-T6 | 0.0254 | 40 | 5.08 | 1.20 |
| 1.0” Al F40-v2 | Al6061-T6 | 0.0254 | Al6061-T6 | 0.0508 | 40 | 2.54 | 0.80 |
| 1.0” Al F40-v3 | Al6061-T6 | 0.04064 | Al6061-T6 | 0.0508 | 40 | 2.54 | 0.82 |
| 1.0” Al F40-v4 | Al6061-T6 | 0.0508 | Al6061-T6 | 0.0508 | 40 | 2.54 | 0.85 |
| 1.0” Al F40-v5 | Al6061-T6 | 0.0508 | Al6061-T6 | 0.08128 | 40 | 2.54 | 0.92 |
| 1.0” Al F40-v6* | Al6061-T6 | 0.0254 | Al6061-T6 | 0.0254 | 40 | 2.54 | 0.73 |

* 3-5% relative density (for all other panels, relative density is 6-8%)

A summary of test conditions and results is given in Table 2. In these tests, failure was defined as the onset of material ejection from the sandwich panel rear facesheet (i.e. detached spall). The test results are defined as: significantly above (>>), above (>), minimally above (≥), equal to (=), minimally below (≤), below (<), and significantly below (<<) the failure threshold. For example, an impact test which results in no visible damage to the panel rear facesheet (i.e. no deformation or bulging) is considered significantly below the failure threshold (<<). A test which results in a central deformation zone and a single pin-sized detached spall or perforation is considered minimally above the failure threshold (≥). Of the 98 impact tests there were 56 pass results and 42 failures.

Table 2. Summary of impact testing

| *Test no.* | *Target* | $d_p$ *(mm)* | $\theta$ *(deg)* | *V (km/s)* | *Result* |
|---|---|---|---|---|---|
| 3147-3[+] | 0.5" Al F10 | 1.2 | 0 | 6.83 | > |
| 3147-4[+] | 0.5" Al F10 | 1.2 | 0 | 6.87 | > |
| 3147-1[+] | 0.5" Al F10 | 1.0 | 0 | 6.95 | < |
| 3147-2[+] | 0.5" Al F10 | 1.1 | 0 | 6.89 | ≤ |
| 3148-1[+] | 0.5" Al F10 | 1.2 | 45 | 7.13 | < |
| 3148-2[+] | 0.5" Al F10 | 1.3 | 45 | 6.9 | < |
| 5045-1[+] | 0.5" Al F10 | 1.4 | 45 | 7.02 | < |
| 3148-3[+] | 0.5" Al F10 | 1.3 | 60 | 6.97 | < |
| 3148-4[+] | 0.5" Al F10 | 1.4 | 60 | 6.85 | < |
| 5045-2[+] | 0.5" Al F10 | 1.5 | 60 | 6.91 | < |
| 5036-3[+] | 0.5" Al F40 | 1.4 | 0 | 6.45 | > |
| 5036-1[+] | 0.5" Al F40 | 1.0 | 0 | 6.88 | < |
| 5036-2[+] | 0.5" Al F40 | 1.2 | 0 | 6.9 | < |
| 8589 | 0.5" Al F40 | 1.3 | 0 | 2.43 | = |
| 5037-2[+] | 0.5" Al F40 | 1.4 | 45 | 6.92 | = |
| 5037-1[+] | 0.5" Al F40 | 1.2 | 45 | 7.05 | < |
| 8571 | 0.5" Al F40 | 1.4 | 45 | 6.68 | < |
| 8572 | 0.5" Al F40 | 2.0 | 60 | 6.7 | ≥ |
| 8582 | 0.5" Al F40 | 2.5 | 60 | 2.63 | ≥ |
| 8580 | 0.5" Al F40 | 1.8 | 60 | 6.79 | ≤ |
| 8581 | 0.5" Al F40 | 2.0 | 60 | 2.28 | << |
| 8261 | 1.0" Al F10 | 2.0 | 0 | 6.87 | ≥ |
| 8280 | 1.0" Al F10 | 2.1 | 0 | 2.18 | > |
| 8269 | 1.0" Al F10 | 2.7 | 45 | 7.04 | > |
| 8268 | 1.0" Al F10 | 2.5 | 45 | 6.62 | << |
| 8272 | 1.0" Al F10 | 3.2 | 60 | 6.7 | > |
| 8252 | 1.0" Al F20 | 2.5 | 0 | 6.88 | > |
| 8253 | 1.0" Al F20 | 2.0 | 0 | 6.85 | ≥ |
| 8276 | 1.0" Al F20 | 2.1 | 0 | 2.46 | > |
| 8254 | 1.0" Al F20 | 1.9 | 0 | 6.87 | << |
| 8425 | 1.0" Al F20 | 2.3 | 0 | 4.71 | < |
| 8255 | 1.0" Al F20 | 2.5 | 45 | 7.1 | > |
| 8257 | 1.0" Al F20 | 2.5 | 45 | 6.46 | ≥ |
| 8256 | 1.0" Al F20 | 2.3 | 45 | 6.88 | < |
| 8259 | 1.0" Al F20 | 3.2 | 60 | 7.1 | ≥ |
| 8258 | 1.0" Al F20 | 3.0 | 60 | 7.13 | ≤ |
| 8260 | 1.0" Al F20 | 3.2 | 60 | 6.68 | << |
| 8263 | 1.0" Al F40 | 2.0 | 0 | 6.52 | ≥ |
| 8279 | 1.0" Al F40 | 3.4 | 0 | 2.62 | >> |
| 8422 | 1.0" Al F40 | 2.5 | 0 | 2.75 | > |
| 8424 | 1.0" Al F40 | 2.3 | 0 | 4.68 | = |
| 8423 | 1.0" Al F40 | 2.1 | 0 | 2.34 | > |
| 9320 | 1.0" Al F40-v3 | 3.0 | 0 | 7 | >> |
| 9321 | 1.0" Al F40-v3 | 2.7 | 0 | 6.94 | = |
| 9322 | 1.0" Al F40-v4 | 2.8 | 0 | 6.59 | ≥ |
| 9323 | 1.0" Al F40-v4 | 2.6 | 0 | 5.88 | = |
| 8567 | 1.0" Al F40 | 1.9 | 0 | 2.2 | << |
| 8568 | 1.0" Al F40 | 2.0 | 0 | 6.63 | << |
| 8585 | 1.0" Al F40 | 2.0 | 0 | 4.43 | << |
| 9072 | 1.0" Al F40 | 2.2 | 0 | 3.11 | < |
| 9073 | 1.0" Al F40 | 2.2 | 0 | 5.36 | << |
| 9074 | 1.0" Al F40 | 2.0 | 0 | 7.56 | << |
| 8420 | 1.0" Al F40 | 2.5 | 45 | 2.44 | = |
| 8569 | 1.0" Al F40 | 2.7 | 45 | 6.66 | > |
| 8270 | 1.0" Al F40 | 2.5 | 45 | 6.78 | << |
| 8271 | 1.0" Al F40 | 2.7 | 45 | 6.99 | < |
| 8421 | 1.0" Al F40 | 2.2 | 45 | 2.68 | < |
| 8427 | 1.0" Al F40 | 2.6 | 45 | 4.78 | << |
| 8428 | 1.0" Al F40 | 2.8 | 45 | 4.76 | << |
| 9075 | 1.0" Al F40 | 2.5 | 45 | 3.76 | << |
| 9065 | 1.0" Al F40 | 2.7 | 45 | 6.7 | < |
| 9066 | 1.0" Al F40 | 2.7 | 45 | 6.86 | < |
| 9067 | 1.0" Al F40 | 2.7 | 45 | 7.11 | < |
| 9068 | 1.0" Al F40 | 2.7 | 45 | 6.79 | < |
| 8267 | 1.0" Al F40 | 3.2 | 60 | 6.57 | << |
| 9007 | 1.0" Al F40 | 3.4 | 60 | 6.91 | < |
| 4161[+] | 2.0" Al F10 | 4.0 | 0 | 6.89 | ≥ |
| 4151[+] | 2.0" Al F10 | 3.6 | 0 | 6.76 | < |
| 4163[+] | 2.0" Al F40 | 4.0 | 0 | 6.79 | ≥ |
| 4152[+] | 2.0" Al F40 | 3.6 | 0 | 6.79 | < |
| 8590 | 2.0" Al F40 | 4.0 | 0 | 2.7 | < |
| 8573 | 2.0" Al F40 | 5.2 | 45 | 6.98 | ≥ |
| 4155[+] | 2.0" Al F40 | 4.0 | 45 | 6.89 | < |
| 4156[+] | 2.0" Al F40 | 4.0 | 45 | 6.84 | < |
| 4162[+] | 2.0" Al F40 | 4.4 | 45 | 6.92 | < |
| 4164[+] | 2.0" Al F40 | 4.4 | 45 | 6.7 | < |
| 5068[+] | 2.0" Al F40 | 4.8 | 45 | 6.93 | < |
| 8613 | 2.0" Al F40 | 7.0 | 60 | 2.73 | > |
| 8591 | 2.0" Al F40 | 5.7 | 60 | 6.74 | < |
| 8614 | 2.0" Al F40 | 6.0 | 60 | 6.74 | < |
| 9220 | 2.0" Al F40 | 6.0 | 60 | 2.74 | ≤ |
| 9324 | 1.0" Al F40-v5 | 3.0 | 0 | 6.71 | > |
| 9357 | 1.0" Al F40 | 2.4 | 0 | 3.25 | < |
| 9358 | 1.0" Al F40 | 2.5 | 0 | 5.48 | > |
| 9359 | 1.0" Al F40 | 2.3 | 0 | 7.38 | > |
| 9360 | 1.0" Al F40 | 2.8 | 45 | 3.52 | > |
| 9362 | 1.0" Al F40 | 2.9 | 45 | 5.50 | < |
| 9363 | 1.0" Al F40 | 2.5 | 45 | 7.19 | ≤ |
| 9374 | 1.0" Al F40-v2 | 2.6 | 0 | 6.66 | < |
| 9376 | 1.0" Al F40-v2 | 3.4 | 45 | 6.72 | > |
| 9377 | 1.0" Al F40-v2 | 3.3 | 45 | 6.85 | > |
| 9325 | 1.0" Al F40-v5 | 2.8 | 0 | 6.91 | ≥ |
| 9326 | 1.0" Al F40-v5 | 3.8 | 45 | 5.80 | ≥ |
| 9327 | 1.0" Al F40-v5 | 3.6 | 45 | 6.83 | > |
| 8574 | 1.0" Al F40-v6 | 2.0 | 0 | 6.63 | ≥ |
| 9375 | 1.0" Al F40-v2 | 2.8 | 0 | 6.64 | ≥ |
| 8575 | 1.0" Al F40-v6 | 3.4 | 60 | 6.88 | < |
| 8583 | 1.0" Al F40-v6 | 2.1 | 0 | 2.10 | < |

[+] Previously reported in 0

### *3.1 Scatter Assessment*

Due to the non-homogeneity of the foam microstructure, the issue of performance scatter may be more relevant for foam core sandwich panels than traditional monolithic-component shields. In order to assess the scatter, a series of six impact experiments were performed at nominally identical conditions (2.7 mm diameter projectile, 45°, 6.8 km/s) on the 1.0" Al F40 target. A comparison of the core and rear wall damage of the six target specimens is made in Fig. 3. Of the six tests, one resulted in perforation (HITF08569) ($d_h$ = 2.0 mm), while the other five showed various degrees of rear wall plastic deformation. Of the non-perforated targets, damage generally extended through ~90% of the foam core thickness, with the exception of HITF09067 (<80%).

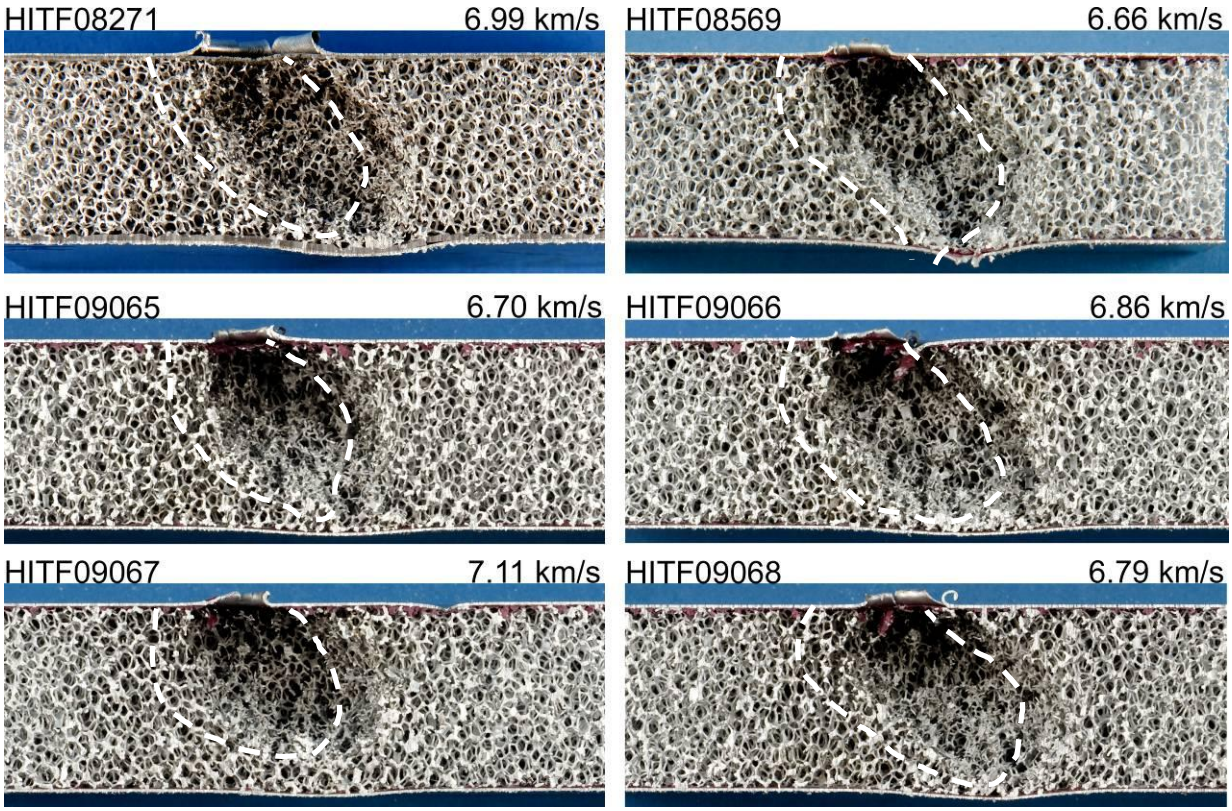


Fig. 3. Comparison of core damage in six targets impacted at nominally-identical conditions (∅ 2.7 mm, 6.8 km/s, 45°).

Although not observed in the Fig. 3 tests, perforation of the sandwich panel rear facesheet from individual fragments penetrating beyond the open cavity of the foam core was a regular occurrence during the test program. This phenomenon, similar to that observed in other porous targets, lead to shield perforation at conditions well below the expected failure limits, complicating the prediction of panel ballistic limits.

### *3.2 The Effect of Pore Density on Shielding Performance*

Three variations of pore density were considered in this study: 10, 20, and 40 PPI. A comparison of the three foam structures is shown in Fig. 4, with details provided in Table 3. To investigate the effect of pore density on shielding performance, a number of tests were performed at nominally identical conditions, a summary of which is given in Table 4.

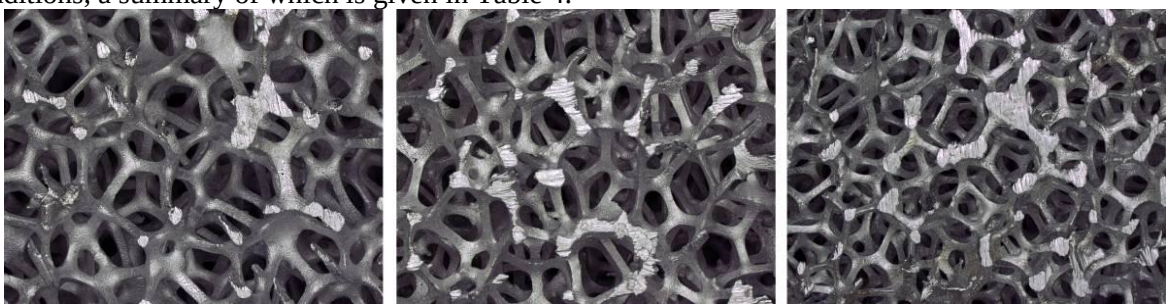

Fig. 4. Comparison of 10 PPI (left), 20 PPI (center), and 40 PPI (right) foam structure (×20 magnification).

Table 3. Characteristic measurements of the three foam cores

| *Pore density* | *Cell size (mm)* | *Pore size (mm)* | *Ligament width ($\mu$m)* |
|---|---|---|---|
| 10 PPI | 3.95 | 2.33 | 382 |
| 20 PPI | 3.28 | 1.78 | 329 |
| 40 PPI | 2.63 | 1.59 | 251 |

Table 4. Comparison of varying PPI shield performance at nominally-identical impact conditions

| *Test no. [10/20/40 PPI]* | *Impact conditions* $\theta$ *(deg)* | $V$ *(km/s)* | $d_p$ *(mm)* | *Result [10/20/40 PPI]* | *Comments* |
|---|---|---|---|---|---|
| 8280/8276/8423 | 0 | 2.18/2.46/2.34 | 2.1 | > / > / > | All targets clearly perforated |
| 8268/8257/8270 | 45 | 6.62/6.46/6.78 | 2.5 | << / ≥ / << | Pin-sized hole in 20 PPI panel |
| 8261/8253/8263 | 0 | 6.87/6.85/6.52 | 2.0 | ≥ / ≥ / ≥ | Small perforation holes in all |
| 8272/8260/8267 | 60 | 6.70/6.68/6.57 | 3.2 | > / << / << | Pin-sized hole in 10 PPI panel |
| 3147-4/-/5036-2 | 0 | 6.87/-/6.90 | 1.2 | > / - / < | Perforation of 10 PPI panel |
| 3148-1/-/5037-1 | 45 | 7.13/-/7.05 | 1.2 | < / - / < | No damage to rear facesheets |
| 5045-1/-/8571 | 45 | 7.02/-/6.68 | 1.4 | < / - / < | Small bulge on 40 PPI panel |
| 4151/-/4152 | 0 | 6.76/-/6.79 | 3.57 | < / - / < | No damage to rear facesheets |
| 4161/-/4163 | 0 | 6.89/-/6.79 | 4.0 | ≥ / - / ≥ | 1/2 holes in 40/10 PPI panel |

Although sensitive to scatter considerations, the shielding performance was found to improve with increasing pore density. A comparison of damages in the 10, 20 and 40 PPI panels impacted at nominally identical conditions is shown in Fig. 5. In the figure, the 10 PPI panel is clearly perforated, while the 20 and 40 PPI panels show minimal bulging. The sectioned cores show that the extension of damage in the 20 PPI panel is deeper than in the 40 PPI panel, progressing through to the rear facesheet.

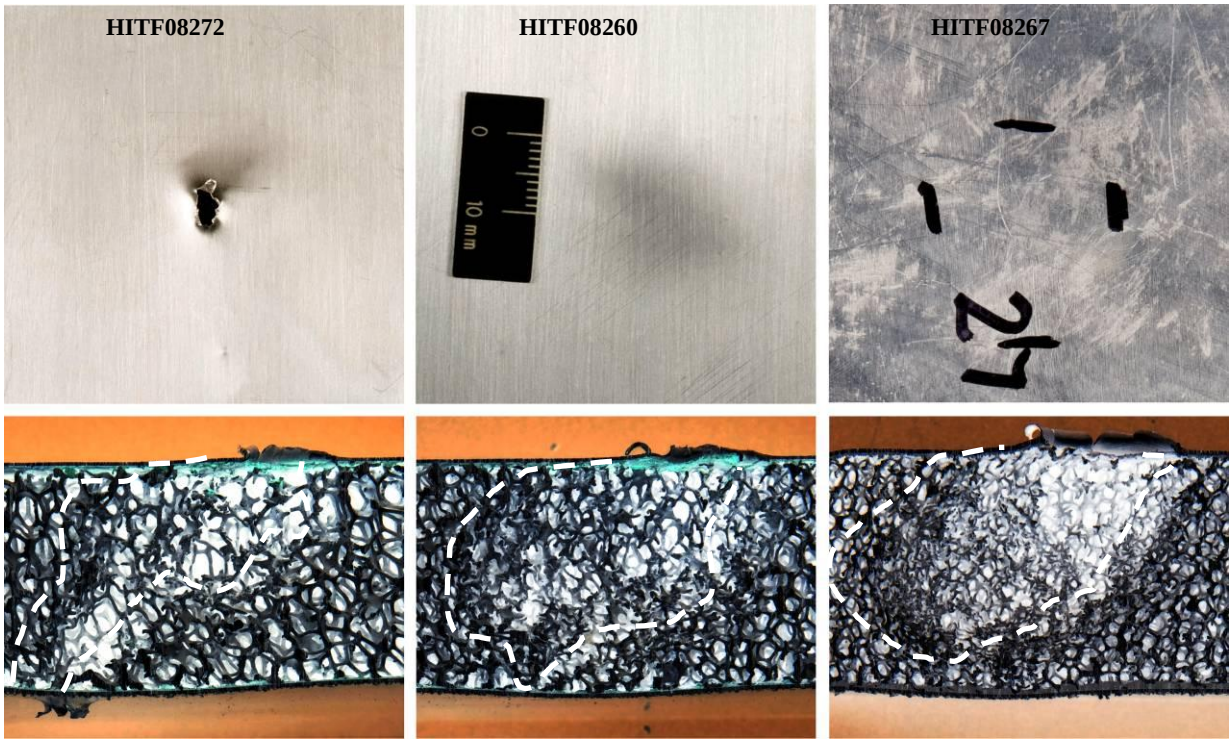


Fig. 5. Comparison of rear facesheet (top) and core (bottom) damages in 1.0" thick 10 (left), 20 (middle), and 40 PPI (right) foam core sandwich panels impacted by 3.2 mm Al2017-T4 diameter spheres at 6.65 ± 0.08 km/s and 60°. Color inversion applied to core images for visualization.

In general, the higher pore density panels seem to be less susceptible to individual solid fragments passing through the core with few or no secondary impacts, leading to perforation cases like that of the 10 PPI panel in Fig. 5. The higher pore density cores also show an increased degree of densification, i.e. collapse of the foam cells, at the limits of the damaged zone, suggesting a greater level of energy partitioning into plastic work (although the effect of this on penetration limits is expected to be minimal). In general, the 40 PPI foam core panels can be considered to perform approximately 5% better than the lower pore density foams (i.e. critical projectile diameter is ~5% larger), however this can often be difficult to differentiate from the experimental scatter.

## 4. The Effect of Relative Density on Shielding Performance

Relative density controls the cross-sectional form of the foam ligaments. In order to investigate this affect on shielding performance, sandwich panels cored with two variations of relative density foam (3-5% and 6-8%), were tested at nominally identical conditions, the results of which are shown in Fig. 6. A 30% decrease in the relative cross-sectional area of the foam ligaments was measured for the 3-5% relative density core, while the cell and pore diameters remained relatively constant.

Although the gross results (i.e. pass/fail) of the three tests shown in Fig. 6 are comparable for both core types, there is a clear increase in the damaged volume of the reduced density foam. For impact of

2.0 mm diameter projectiles at ~6.8 km/s and 0°, the penetration depth into the 3-5% panel is clearly greater than for the 6-8% panel, while for impact of 3.4 mm projectiles at 60°, the damage volume is substantially larger. The 3-5% core panels have an average areal density of 0.66 g/cm$^2$, approximately 12% less than the baseline 6-8% relative density panels. It is expected that the variance in penetration depth and damage expansion is due predominantly to the weight of the foam core rather than the variation in characteristic structure (i.e. change in ligament shape).

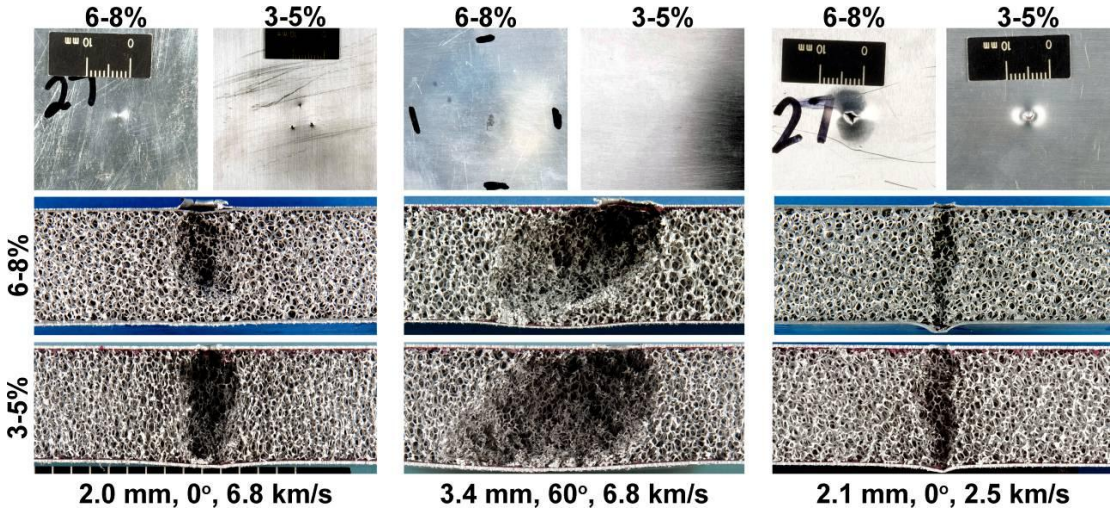


Fig. 6. Comparison of rear facesheet (top) and core damages in 1.0" thick panels with 6-8% and 3-5% relative core density.

## 5. A Ballistic Limit Equation for Foam Core Sandwich Panels

A ballistic limit equation (BLE) based on the new non-optimum Whipple shield equation (NNO) 0 was derived for the foam core sandwich panels. In the low velocity regime, i.e. $V \le V_{LV}$,

$$d_c = \frac{1.83\left(t_b + t_w\left(\sigma/40\right)^{0.5} + {t_f}^{1.1}\left(\rho_f/\rho_w\right)\right)}{\left({\rho_p}^{0.5}\cdot V^{2/3}\cdot\left(\cos\theta\right)^{4/5}\right)^{18/19}} \quad (1)$$

where $t_b$ is the front facesheet thickness (cm), $t_w$ is the rear facesheet thickness (cm), $\sigma$ is the rear facesheet yield strength (ksi), $t_f$ is the foam core thickness (cm), $\rho_f$ is the volumetric density of the foam core (g/cm$^3$), $\rho_w$ is the rear facesheet material density (g/cm$^3$), $\rho_p$ is the projectile material density (g/cm$^3$), V is velocity (km/s), $\theta$ is the impact angle measured normal to the target surface (deg), and $d_c$ is the critical projectile diameter. Eq. (1) includes the effect of the foam core in the maximum allowable penetration depth via determination of an equivalent aluminum plate thickness based on near-linear density scaling. Additionally, angle dependence is increased to $(\cos\theta)^{4/5}$ from the NNO relationship.

Secondary impacts of projectile and bumper fragments on individual foam ligaments have been

found to increase the thermal state of penetrating particles, leading to fragmentation, melt, and vaporization at lower impact velocities than traditional shields (e.g. 0). As such,

$$V_{LV} = 2.25 \Big/ \left(\cos\theta\right)^{1/3} \tag{2}$$

In the hypervelocity regime, i.e. $V \geq V_{HV}$,

$$d_c = 2.152 \frac{\left(t_w + 0.5\,AD_f/\rho_w\right)^{2/3} 0.89 \cdot t_f{}^{0.45} \left(\sigma/70\right)^{1/3}}{\rho_p{}^{1/3} \rho_b{}^{1/9} V^{2/5} \cos\theta^{4/5}} \tag{3}$$

where $AD_f$ is the foam core areal density (g/cm$^2$) and $\rho_b$ is the density of the front facesheet material. The effect of the foam core is included through an increase in the rear wall thickness corresponding to 50% of an equivalent areal weight plate, and an increase in core thickness (or facesheet spacing, $S$) dependence from 1/3 to 0.45. The transition from shatter-to-hypervelocity regime ($V_{HV}$) is considered to occur once an increase in projectile velocity results in increased penetration depth and, hence, rear facesheet damage, defined as:

$$V_{HV} = 4.0 \Big/ \left(\cos\theta\right)^{1/3} \tag{4}$$

It should be noted that extrapolation to hypervelocities is performed at a rate above kinetic energy scaling due to the availability of test data in the (defined) hypervelocity regime.

In the intermediate regime, i.e. $V_{LV} < V < V_{HV}$, linear interpolation is applied:

$$d_c = d_c\left(V_{LV}\right) + \frac{\left(d_c\left(V_{HV}\right) - d_c\left(V_{LV}\right)\right)}{V_{HV} - V_{LV}} \times \left(V - V_{LV}\right) \tag{5}$$

The ballistic limit equation is derived for application with 40 PPI foam core panels. As described previously, the performance of the 40 PPI foams was found to be superior to that of the 20 and 10 PPI panels. As such, a nominal 5% decrease in the predicted critical projectile diameter in the hypervelocity regime should be applied for application of the BLE to 10 and 20 PPI core panels.

In Fig. 7 the ballistic limit equation is expressed as a curve, demarcating between impact conditions expected to lead to failure of the structural panel, and those against which the shield is capable of defending. Test data is also included in the figures. Of the 98 impact tests reported in Table 2, 70 (71%) are predicted accurately, 25 tests (26%) are slightly conservatively predicted (i.e. $d_p/d_c < 1.2$), two (2%) are conservatively predicted ($d_p/d_c < 1.5$) and one (1%) is non-conservatively predicted. However, the non-conservative prediction is within 0.3% of the test value (i.e. $d_p/d_c > 99.7\%$), which is considered well within the experimental scatter bounds. In Fig. 8 the predictions of the BLE are plotted in terms of $d_p/d_c$ ratio for all the test data reported in Table 2.

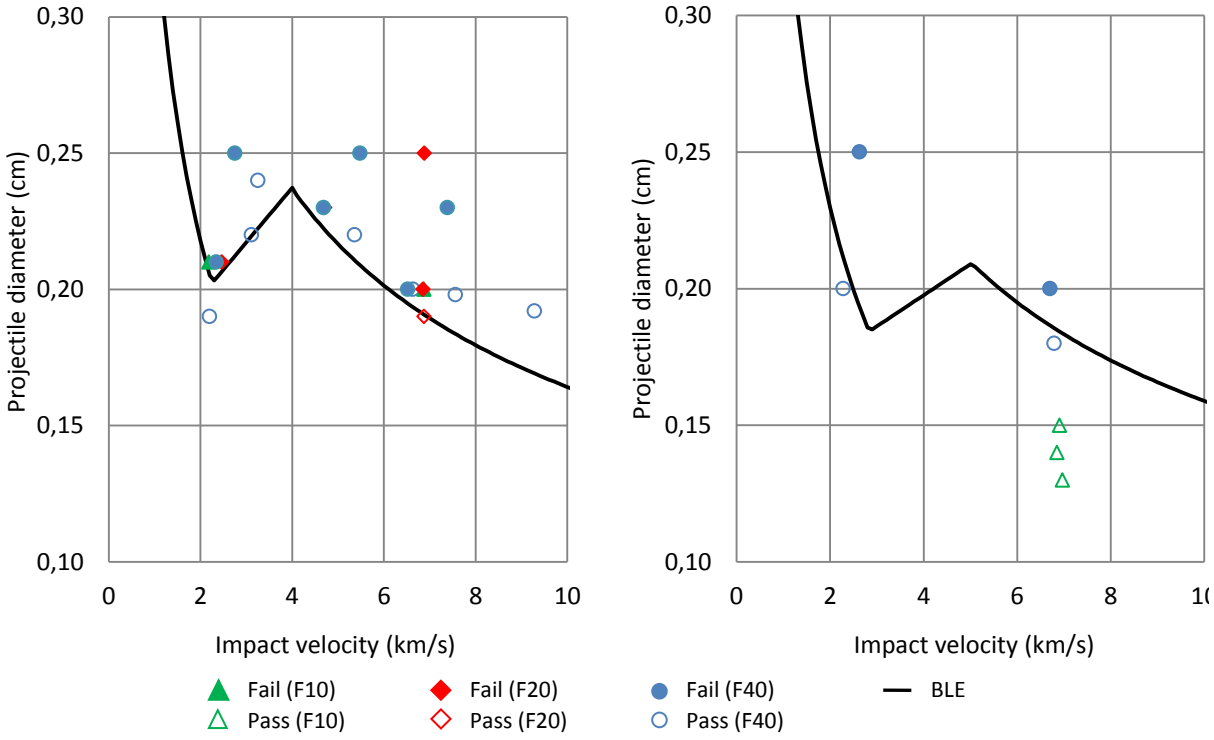


Fig. 7. Ballistic limit curve for the 1.0" Al F40 sandwich panel at normal incidence (left) and 60° (right).

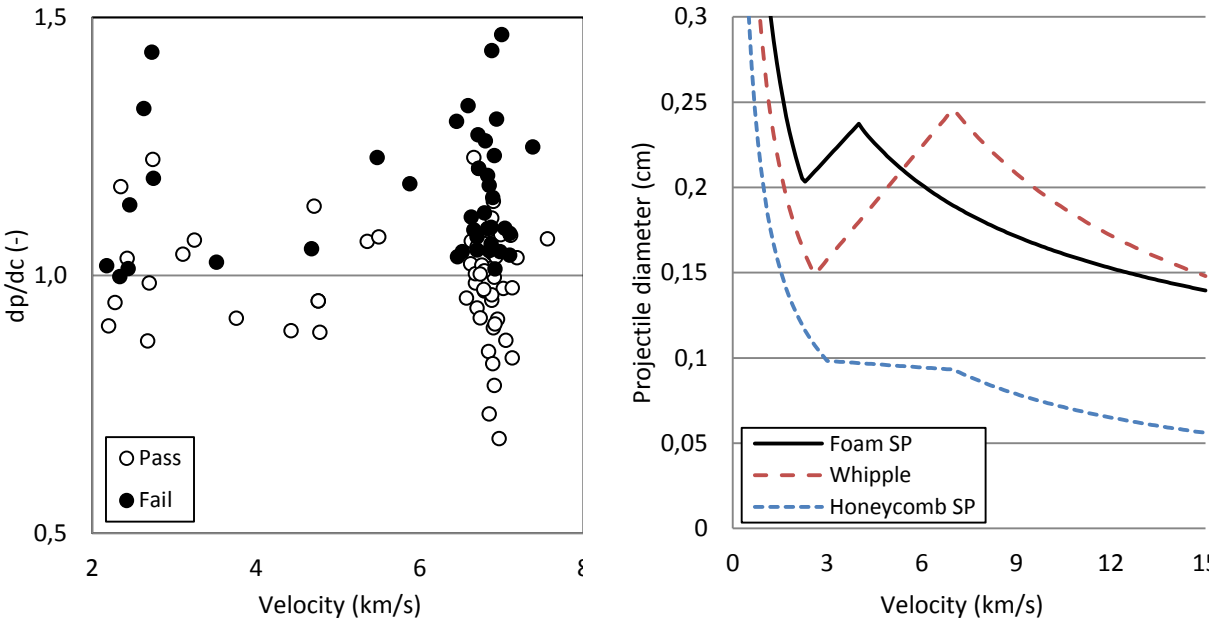


Fig. 8. Summary of the BLE predictions (left) and comparison of the foam SP BLE with traditional shield types (right).

## 6. Comparison to Traditional Shielding Configurations

In order to evaluate the shielding performance of the foam core sandwich panels, the derived ballistic limit equation can be compared to those of other common shield types. In Fig. 8 the foam BLE is plotted against flight-representative examples of a metallic Whipple shield (BLE from 0) and aluminum honeycomb sandwich panel (BLE from 0). The Whipple shield evaluated consists of a 0.07 cm thick Al6061-T6 bumper and 0.18 cm thick Al6061-T6 rear wall, with a total areal density of 0.69 g/cm$^2$. The honeycomb sandwich panel has 0.105 cm thick Al6061-T6 facesheets, with a type 1/8-5052-.001 honeycomb core (volumetric density = 0.072 g/cm$^3$) for a total areal density of 0.75 g/cm$^2$. The total thickness of the panels is maintained at 2.54 cm. It should be noted that the Whipple shield curve is de-rated according to additional non-ballistic mass required for the shield support structure, which is approximated as 30% of the bumper mass 0.

The foam sandwich panel is shown to perform better than the aluminum honeycomb sandwich panel over the range of velocities considered. At velocities below 5 km/s, the performance of the foam panel is also superior to that of the metallic Whipple shield, yet poorer at higher velocities. The differing velocity dependence of the Whipple and foam BLEs is demonstrated by the decrease in performance variation between the two shields in the hypervelocity regime. It is expected that for mission risk assessment, the foam sandwich panel and Whipple shield configurations would provide comparable results.

## 7. Summary and Conclusions

Metallic open cell foams are of interest for micrometeoroid/debris shielding as they provide comparable mechanical and thermal performance to traditional structures such as honeycomb sandwich panels without MMOD-shielding detrimental though-thickness channeling cells. Preliminary investigations have demonstrated the potential of these structures in complex configurations (e.g. double layer foam bumpers 0). In this study, 90 hypervelocity impact tests were performed on open cell foam core sandwich panel structures, with varying impact conditions (velocity, angle, projectile diameter) and target configurations to characterize the effect of design variables such as pore size, relative density, core thickness, and facesheet thickness on shielding capability. From the test results, shielding performance was found to increase (albeit minimally) with increasing pore density. Furthermore, secondary impacts of projectile and front facesheet fragments on individual foam ligaments were considered to induce fragmentation, melt, and vaporization at lower velocities than traditional shielding configurations due to increased thermal energy from the non-isentropic shock and isentropic release processes. A ballistic limit equation, based on the new non-optimum Whipple shield BLE 0 was derived for the foam core structures for use in risk assessment tools such as BUMPER. The equation was accurate for 71% of the test results, conservative for 28%, and non-conservative for a single test (1%). However, the non-conservative prediction was within 0.3% of the projectile diameter in the failed test, which is considered to be well within the limits of experimental scatter. The low-to-shatter, and shatter-to-hypervelocity regime limits of the BLE were defined at 2.25 km/s and 4.0 km/s for normal impact respectively, reflecting the enhanced thermal heating effects of repeated shocking from secondary impacts on the foam structure.

The performance of the foam core sandwich panels was compared against that of typical lightweight MMOD shields, taking into account support requirements for non-structural

configurations (i.e. non-ballistic mass). The foam panel was shown to perform significantly better than aluminum honeycomb core sandwich panel over the range of velocities considered (0-15 km/s), demonstrating the potentially substantial protection enhancement possible for vehicles without a dedicated protective structure. The performance of the foam panel was superior to that of the scaled Whipple shield at velocities below 5 km/s, above which the Whipple shield was superior. The panels tested are not intended to replace heavy, dedicated protective systems (such as the stuffed Whipple shield) for large vehicles, or missions operating in highly polluted orbits (e.g. 800-1000 km altitude). However, for unmanned missions, or vehicles with extreme weight or volume restrictions, the open cell foam core sandwich panel structure represents a feasible new alternative. Furthermore, we consider that optimization of these structures may lead to sizeable improvements in protective capability and efficiency.

## Acknowledgements

All testing was performed at the NASA JSC White Sand's Test Facility in Las Cruces, NM.

## References

[1] Sennett R, Lathrop B. Effects of hypervelocity impact on honeycomb structures. *Journal of Spacecr*aft, 1968; 5(12): 1496-1497.

[2] Destefanis R, Schäfer F, Lambert M, Faraud M. Selecting Enhanced Space Debris Shields for Manned Spacecraft. *Int. J. of Impact Eng.* 2006; 33: 219-230.

[3] Ryan S, Hedman T, Christiansen E. Honeycomb vs. foam: evaluating a potential upgrade to International Space Station module shielding for micrometeoroids and orbital debris, NASA Johnson Space Center, Houston, 2009, NASA/TM-2009-214793.

[4] Yasensky J, Christiansen E. Hypervelocity impact evaluation of metal foam core sandwich structures, NASA Johnson Space Center, Houston, 2008, NASA/TP-2008-214776.

[5] Christiansen E. Design and performance equations for advanced meteoroid and debris shields. *Int. J. of Impact Eng.* 1993; 14: 145-156.

[6] Ryan S, Bjorkman M, Christiansen E. Characteristics of Whipple shield performance in the shatter regime, submitted for publication at HVIS 2010 (abstract no. 77).

[7] Ryan S, Christiansen E. Micrometeoroid and orbital debris (MMOD) shield ballistic limit analysis program, NASA Johnson Space Center, Houston, 2009, NASA/TM-2009-214789.

[8] Christiansen E. Meteoroid/Debris Shielding, NASA Johnson Space Center, Houston, 2003, TP-2003-210788.